Wind-driven ocean influences on the contrasting sea-ice trends around West Antarctica

Sang-Ki Lee[1], Denis L. Volkov[2,1], Hosmay Lopez[2,1], Woo Geun Cheon[3], Arnold L. Gordon[4], Yanyun Liu[2,1] and Rik Wanninkhof[1]

[1]Atlantic Oceanographic and Meteorological Laboratory, NOAA, Miami, FL

[2]Cooperative Institute for Marine and Atmospheric Studies, University of Miami, Miami, FL

[3]The 6th R&D Institute-1, Agency for Defense Development, Changwon, Republic of Korea

[4]Lamont-Doherty Earth Observatory, Earth Institute at Columbia University, Palisades, New York, USA

Submitted to Journal of Geophysical Research

October 2016

Corresponding author address: Dr. Sang-Ki Lee, NOAA, Atlantic Oceanographic and Meteorological Laboratory, 4301 Rickenbacker Causeway, Miami, FL 33149, USA.

E-mail: Sang-Ki.Lee@noaa.gov.

Abstract

Since late 1978, Antarctic sea-ice extent in the East Pacific has retreated persistently over the Amundsen and Bellingshausen Seas in warm seasons, but expanded in cold seasons, while an almost opposite trend has occurred in the Atlantic. Previous studies have shown that the contrasting sea-ice trends in the East Pacific and Atlantic could be explained by the strengthening Southern Hemisphere (SH) subpolar low over West Antarctica and associated cold- and warm-air advections and sea-ice drift. By using a surface-forced ocean and sea-ice coupled model, here we show that wind-driven ocean processes also played a key role. In the East Pacific, the strengthening SH westerlies in the region enhanced Ekman upwelling of the warm upper Circumpolar Deep Water, which directly contributed to the retreat of sea-ice in warm seasons, and increased the northward Ekman transport of cold Antarctic surface water, which supported the expansion of sea-ice in cold seasons. In the Atlantic, the northern branch of the Weddell Gyre strengthened due to the poleward intensification of SH westerlies in the region. This in turn sharply increased the meridional thermal gradient across it as constrained by the thermal wind balance. The associated cooling within the Weddell Gyre and warming to the north contributed to the expansion of sea-ice within the Weddell Gyre in warm seasons, and the retreat to the north in cold seasons. A positive feedback involving sea-ice, air-sea heat flux and surface ocean temperature further amplified the changes in Antarctic sea-ice extent during warm seasons.

1. Introduction

The satellite passive microwave data record since late 1978 shows that the Antarctic sea-ice extent has overall expanded in all seasons [e.g., Turner and Overland, 2009], in stark contrast to the retreating Arctic sea-ice extent [e.g., Stroeve et al., 2012]. Several studies have suggested that the surface freshening and enhanced salinity stratification in the Antarctic seas, caused by the melting of the Antarctic glaciers and ice-sheet related to anthropogenic global warming, suppressed convective mixing with the warmer water at depth and thus inhibited the melting of Antarctic sea-ice overall [e.g., Bintanja et al., 2015; de Lavergne et al., 2014; Bintanja et al., 2013; Zhang, 2007]. However, around West Antarctica, the trend is not homogeneous throughout the seasons or the longitudes [e.g., Parkinson and Cavalieri, 2012]. In particular, as shown in Figures 1a and b, Antarctic sea-ice extent in the East Pacific (150°W - 60°W) has retreated substantially over the Amundsen and Bellingshausen Seas during the warm seasons from December to May (DJFMAM), but expanded during the cold seasons from June to November (JJASON). In the Atlantic (60°W - 0°), on the other hand, Antarctic sea-ice extent has expanded over the Weddell Sea during the warm seasons, but retreated during the cold seasons (see Figure 2 that shows the oceans and regional seas around Antarctica).

Antarctic sea-ice is intimately coupled to the atmosphere-ocean processes over the Southern Ocean. For example, the expansion and retreat of Antarctic sea-ice exert a major control on surface albedo and thus the atmospheric radiative energy balance [e.g., Ebert and Curry, 1993; Walsh, 1983]. Antarctic sea-ice insulates the underlying ocean from the air-sea fluxes of heat, momentum and carbon. Therefore, its long-term trend could either slow down or accelerate ocean warming and acidification (see Wanninkhof et al. [2013] and Takahashi et al. [2009] for the global ocean carbon uptake, and Rysgaard et al. [2011] for the Antarctic sea-ice contribution to the air-sea CO_2 flux in the Southern Ocean), and thus potentially modulate the Southern Ocean's response to the increasing anthropogenic greenhouse gases. Additionally, Antarctic sea-ice affects the availability of food and shelter for Antarctic krill (*Euphausia superba*), the key species in the Antarctic marine food web, during the early life stages and thus impacts their survival [e.g., Piñones and Fedorov, 2016; Brierley et al., 2002; Meyer et al., 2002].

Various hypotheses have been proposed to explain the spatially and seasonally inhomogeneous trend of sea-ice extent around West Antarctica. Several studies have suggested that the positive trend of the Southern Annular Mode (SAM) during the past decades, due to ozone depletion and increasing greenhouse gases [e.g., Lee and Feldstein, 2013; Son et al., 2008; Shindell and Schmidt, 2004; Gillett and Thompson, 2003], and El Niño-Southern Oscillation (ENSO) teleconnections, and their influences on wind-driven surface heat flux are mainly responsible for the observed sea-ice trends [e.g., Matear et al., 2015; Ding et al., 2011; Stammerjohn et al., 2008; Yuan and Li, 2008; Liu et al., 2004; Yuan, 2004; Kwok and Comiso, 2002; Renwick, 2002]. Many of these studies also pointed out that wind-driven surface heat flux alone is insufficient to explain the magnitude and the spatiotemporal pattern of the observed Antarctic sea-ice trend [e.g., Liu et al., 2004]. For instance, Holland and Kwok [2012] argued that wind-driven changes in sea-ice drift are the main driver of the sea-ice trends around West Antarctica during 1992 - 2010, while Matear et al. [2015] suggested that anthropogenic warming is required to explain the observed sea-ice retreat in the Amundsen and Bellingshausen Seas since 1979.

A recent study by Clem and Renwick [2015] suggested that the increasing tendency of atmospheric convection over the South Pacific Convergence Zone forced stationary Rossby waves to strengthen the Southern Hemisphere (SH) subpolar low over West Antarctica, which in turn could bring cold Antarctic air northward over the East Pacific and warm subtropical air southward over the Atlantic. This hypothesis is indeed consistent with the increasing Antarctic sea-ice fraction in the East Pacific and the decreasing Antarctic sea-ice fraction in the Atlantic during the cold seasons (Figure 1b), although it does not explain the opposite trends during the warm seasons (Figure 1a). Meehl et al. [2016] proposed a similar hypothesis to suggest that the increasing Antarctic sea-ice extent during 2000 - 2014, the period known as the global warming hiatus [e.g., Meehl et al., 2011], is linked to the negative phase of the Interdecadal Pacific Oscillation (IPO). Purich et al. [2016] used coupled model simulations to present a consistent result. They stressed that the phase change in the IPO from positive to negative over 1979-2013 contributed to the observed strengthening of the SH subpolar low over the Amundsen Sea and the associated cold- and warm-air advections, thereby increasing the sea-ice in the Ross Sea and decreasing in the Bellingshausen Sea. Founded on a similar mechanism, Li et al. [2014] proposed that warm tropical North Atlantic sea surface temperatures (SSTs), associated with the Atlantic Multidecadal Oscillation (AMO) [Enfield et al., 2001], could produce interhemispheric teleconnections [Ji et al., 2014; Simpkins et al., 2014; Lee et al., 2013; Wang et al., 2010] to strengthen the SH subpolar low over the Amundsen Sea. This could in turn melt the sea-ice over the Antarctic Peninsula by warm-air advection and increase the sea-ice over the Ross Sea by cold-air advection. Zhang et al. [2016], using a fully coupled climate model, also reported that North Atlantic SSTs could influence the changes in Antarctic sea-ice extent emphasizing the Atlantic Meridional Overturning Circulation as the main driver.

Previous studies, as discussed above, have collectively shown that changes in local winds, induced by the positive trend of SAM and stationary Rossby waves emanating from the tropical Pacific and Atlantic, together with a warming-induced surface freshening, caused the spatially and seasonally inhomogeneous sea-ice trend around West Antarctica. They stressed wind-driven surface heat fluxes (i.e., warm- and cold-air advections) and sea-ice transport, and enhanced salinity stratifications, as the key forcing mechanisms. However, in many of these studies the potential role of wind-driven ocean thermal and dynamic processes were either neglected or not fully incorporated, partly due to the scarcity of in-situ ocean observations in the Antarctic seas [e.g., Legler et al., 2015; Rintoul et al., 2012]. Since both the atmosphere and ocean processes are involved in the seasonal formation and melting of Antarctic sea-ice [e.g., Gordon and Taylor, 1975], it is likely that regional ocean thermal and dynamic processes played an important role in shaping the spatially and seasonally inhomogeneous sea-ice trend around West Antarctica. Therefore, our main goal in this study is to investigate if and how the recent trends of West Antarctic sea-ice were affected by regional ocean thermal and dynamic processes. To achieve this goal, here we utilize satellite-derived sea-ice data and a surface-forced ocean and sea-ice coupled model to present potential mechanisms involving ocean thermal and dynamic processes that have not been fully explored, but could further explain the inhomogeneous sea-ice trends around West Antarctica during the recent decades.

Section 2 describes the observational data, the model, and the model experiments that were utilized. Section 3 shows the modeled sea-ice trends around West Antarctica and compares them with the observations. Then, the model results for the East Pacific (150°W - 60°W) and Atlantic

(60°W - 0°) are analyzed in section 4 and 5, respectively. Based on these analyses, three processes (or mechanisms), namely (1) Ekman heat transport and upwelling, (2) the strength of the Weddell Gyre, and (3) a positive feedback involving sea-ice, air-sea heat flux and surface ocean temperature, are presented as key contributing factors to the inhomogeneous sea-ice trends around West Antarctica. Section 6 further presents and discusses the interannual variability of Antarctic sea-ice around West Antarctica by using the leading Empirical Orthogonal Function (EOF) modes of detrended Antarctic sea-ice variability. Section 7 provides a summary and discussion.

2. Data and Model Experiments

The Hadley Center sea-ice and SST data sets [Rayner et al., 2003] were used to derive monthly observed sea-ice fraction data for the period of 1979 - 2014. The monthly sea-ice fraction data were reconstructed by blending and adjusting all available digitized sea-ice data including the passive microwave satellite data from late 1978 onward measured from several sensors [Rayner et al., 2003]. There is no reliable long-term in-situ ocean observation system in place in the Antarctic seas [Legler et al., 2015; Rintoul et al., 2012]. Therefore, we used the global ocean and sea-ice coupled model of the NCAR Community Earth System Model version 1 (CESM1; Danabasoglu et al., 2012) forced with the Modern-Era Retrospective analysis for Research and Applications (MERRA; Rienecker et al., 2011) surface flux fields for the period of 1979 - 2014 in order to reproduce the observed Antarctic sea-ice trends and to further explore the role of ocean thermal and dynamic processes.

The ocean component of CESM1 is based on the Parallel Ocean Program version 2, [Danabasoglu et al., 2012]. The sea-ice component of CESM1 is based on the Community Ice Code version 4, which is a dynamic-thermodynamic model that treats the ice pack as a flow-dependent elastic-viscous-plastic material [Hunke and Lipscomb, 2008]. The ocean model is divided into 60 vertical levels. Both the ocean and sea-ice model components have 360 longitudes and 384 latitudes on a displaced pole grid, with a longitudinal resolution of about 1.0° and a variable latitudinal resolution of approximately 0.3° near the equator. An important advancement in CESM1 from earlier versions is the specification of a spatially variable coefficient in the Gent and McWilliams eddy parameterization, rather than a constant value; the ocean response (e.g., strengthening of the Antarctic Circumpolar Current) to increasing SH winds is in reasonable agreement with experiments using ocean models with much higher resolution that do not use this eddy parameterization [Gent and Danabasoglu, 2011]. Danabasoglu et al. [2012] provide a more detailed description of the CESM1 ocean model. See Landrum et al. [2012] for the CESM1 simulation of Antarctic sea-ice climatology.

To spin up the ocean and sea-ice coupled CESM1, it was initialized using temperature and salinity fields obtained from the polar hydrographic climatology [Steele et al., 2001] and integrated for 400 years using the 20th century reanalysis (20CR) surface flux fields from the period of 1948 - 1977 [Compo et al., 2011]. In the spin-up run, the 6-hourly surface wind vectors, air temperature and specific humidity, daily shortwave and downward longwave radiative heat fluxes, and monthly precipitation rate were specified. The upward longwave radiative heat flux and turbulent surface fluxes were determined interactively by using the 6-hourly surface wind speed, air temperature and specific humidity, along with the modelproduced SSTs. To incorporate the impact of atmospheric noise during the spin-up, which plays a crucial role especially in thermohaline convection and deep-water formation in the North Atlantic sinking regions [e.g., Wu et al., 2016; Kirtman et al., 2012], the surface forcing fields in each model year were randomly selected from the period of 1948 - 1977, following the spin-up methodology used in Lee et al. [2011] and others [e.g., Liu et al., 2015; Lee et al., 2015]. In the spin-up run and also in other runs, the long-term mean values of freshwater discharge from continents derived from Dai and Trenberth [2002] were prescribed. A constant freshwater flux of 0.073 Sv (10^6 m^3s^{-1}), which was derived based on a freshwater flux budget of the Southern Ocean [Large and Yeager, 2009], was uniformly distributed along the Antarctic coast - Jacobs et al. [1992] estimated a slightly larger value of 0.083 Sv.

After the 400 years of the spin-up run, the 20CR surface flux fields were used to force CESM1 for the period of 1948 - 1978, while the MERRA surface flux fields were used to continue the model run for 1979 - 2014. Note that the 20CR surface flux fields were corrected (i.e., monthly climatologies and 5-day high-pass filtered) by using the surface flux fields obtained from the common ocean–ice reference experiments version 2 [Large and Yeager, 2009]. Additionally, to ensure a smooth transition of the model simulation during the late 1970s, the MERRA climatological surface flux fields were adjusted to match the bias-corrected 20CR climatological surface flux fields. The 36-year ocean and sea-ice coupled CESM1 simulation forced with the adjusted MERRA surface flux fields is referred to as the control simulation.

3. West Antarctic Sea-Ice Trends in CESM1 Control Simulation

The linear trends in Antarctic sea-ice fraction over the period of 1985 - 2014 for the warm and cold seasons obtained from the control simulation are shown in Figures 1c and d, respectively. Note that the first six years (1979 - 1984) of the model results were excluded to prevent any potential model drift in the beginning of the control simulation from affecting the modeled sea-ice trend (hereafter, a linear trend in any variable multiplied by 35 years is simply referred to as a trend or a linear trend). Overall, the control simulation reasonably reproduced the spatial patterns of Antarctic sea-ice trend for both the warm and cold seasons, such as the largely decreasing Antarctic sea-ice fraction over the East Pacific in the warm seasons and over the Atlantic in the cold seasons, although it did not well reproduce the increasing Antarctic sea-ice fraction over the West Pacific. Since the linear trends of West Antarctic sea-ice fraction are regionally coherent within the East Pacific (150°W - 60°W) and within the Atlantic (60°W - 0°), and reasonably reproduced in the control simulation, the linear trends of West Antarctic sea-ice fraction are zonally averaged and explored for each of the regions in the following sections.

4. Antarctic Sea-Ice Trend in the East Pacific

Figures 3a and b show the linear trends of Antarctic sea-ice fraction averaged over the East Pacific for each calendar month obtained from the control simulation and the observations, respectively. The two green lines in each panel represent 5 and 90% climatological sea-ice fractions. Although the control simulation underestimates the decreasing sea-ice fraction in the warm seasons and overestimates the increasing sea-ice fraction in the cold seasons, the model reasonably well reproduced overall the spatiotemporal pattern of Antarctic sea-ice trend in the East Pacific. It should be noted that the changes in Antarctic sea-ice fraction over the East

Pacific during the recent decades occurred mainly in the outer edge of sea-ice (i.e., between 5 and 90% sea-ice fraction), while the inner-core (i.e., greater than 90% sea-ice fraction) that mainly forms in the cold seasons was nearly unaffected.

To address if and how ocean processes affected the seasonally distinctive Antarctic sea-ice trends over the outer edge in the East Pacific, we first looked at the linear trends of ocean temperature zonally averaged over the East Pacific. As shown in Figures 4c and d, the upper ocean temperatures north of 68°S decreased considerably (up to -1.0°C) in both the cold and warm seasons in line with the increasing sea-ice fraction in the outer edge during the cold seasons (Figure 4b). This suggests that the colder upper ocean temperatures favored the increased sea-ice fraction in the outer edge in the cold seasons (i.e., larger surface ocean area at temperatures below freezing point). Note that the opposite scenario (i.e., the increased sea-ice fraction affecting the upper ocean temperatures in the cold seasons) should have resulted in warmer upper ocean temperatures (i.e., due to smaller ocean area exposed to the seasonal surface cooling). As shown in Figure 5a, the year-round cooling trends of the upper ocean north of 68°S (Figures 4c and d) are largely driven by the increasing northward advection of cold Antarctic surface water (see Talley et al. [2011] for the water mass distribution in the Southern Ocean). The increasing northward velocity in the upper 100 m matches quite well with the overall positive trends of zonal wind stress (τ_x) and the implied Ekman transport. This suggests that the increasing northward advection of cold Antarctic surface water is driven by the increasing SH westerlies over the East Pacific enabled by the strengthening SH subtropical high and SH subpolar low in the region (Figures 6a and b).

Perhaps, the most striking feature in the ocean temperature trends of the East Pacific (Figures 4c and d) is the large warming of subsurface water between 100 and 300 m (up to 0.9°C). The subsurface warming south of around 65°S is largely due to the enhanced regional upwelling of the warm upper Circumpolar Deep Water (CDW) - the climatological ocean temperatures are warmer with depth in this region because the upper ocean is relatively fresh and exposed to cold Antarctic air. Indeed, as shown in Figure 5b, the outer edge of sea-ice is exposed to the year-long Ekman upwelling trend, induced by the negative wind stress curl tendency associated with the increasing SH westerlies over the East Pacific (Figures 6a and b). The subsurface warming and the concurrent decrease in the sea-ice south of 68°S in the warm seasons (see Figures 4a and c) suggest that the warm upper CDW is responsible for (or at least contributed to) the melting sea-ice in the warm seasons, which is possible during austral fall in March - May (MAM) when the surface mixed layer deepens. More specifically, the seasonal cooling at the surface and seasonally enhanced vertical mixing in austral fall could entrain the warm upper CDW to increase the mixed layer temperature and thus slow down (or disrupt) the seasonal formation of sea-ice. In austral spring and summer, the surface layer is too stratified and stable to bring the warm upper CDW to the surface.

It is interesting to note that the subsurface warming also prevails during the cold seasons (Figure 3d). However, it has little impact on the sea-ice in the inner core during the cold seasons because the surface water in the inner core is almost completely insulated from cold Antarctic air, thus preventing vertical mixing, which is required to bring the warm upper CDW to the surface and melt the sea-ice. Consistent with this reasoning, the surface ocean temperatures south of 68°S did not change appreciably in the cold seasons (Figure 4d).

The above analysis suggests that the enhanced Ekman upwelling of the warm upper CDW and the increased northward cold water transport in the East Pacific, driven by the increasing SH westerlies in the region, changed the surface ocean temperatures in the outer edge and thus the sea-ice fraction. However, air-sea heat flux could also affect the surface ocean temperatures in the outer edge and thus the sea-ice fraction, and be affected by the changing sea-ice fraction. Figure 5c shows the linear trends of net air-sea heat flux (positive downward) and Antarctic sea-ice fraction, both averaged over the East Pacific for each calendar month, derived from the control simulation. Over the outer edge of sea-ice, the seasonal surface cooling in June - September tends to weaken (i.e., surface heating trend), which is a response to the increased sea-ice fraction in the region (i.e., due to smaller ocean area exposed to the seasonal surface cooling). On the other hand, the seasonal surface cooling in austral fall (MAM) tends to strengthen (i.e., surface cooling trend) over the outer edge in response to the decreasing sea-ice fraction (i.e., due to larger ocean area exposed to the seasonal surface cooling). During the months of November - January, the seasonal surface warming tends to weaken over the area of decreasing sea-ice fraction south of 70°S and intensify over the area of increasing sea-ice fraction north of 70°S, both in response to the regional changes in the sea-ice fraction.

The air-sea heat flux trends over the outer edge of sea-ice in the East Pacific represent a response rather than a driver. There is a negative feedback involving sea-ice, air-sea heat flux and surface ocean temperature during the months of climatological surface cooling in March - September (e.g., an increased sea-ice fraction could lead to surface ocean warming, which could in turn decrease sea-ice fraction), and a positive feedback during the short window of climatological surface warming in November - January (e.g., an increased sea-ice fraction could lead to surface ocean cooling, which could in turn further increase sea-ice fraction). This positive feedback appears to be a contributing factor to the large surface warming trend south of 70°S during the warm seasons (Figure 4c).

5. Antarctic Sea-Ice Trend in the Atlantic

As indicated in Figures 3c and d, the inner core of Antarctic sea-ice in the Weddell Sea is almost unaffected, in agreement with the earlier reports that the Weddell Polynya of the mid-1970s has not repeated afterward [e.g., Gordon et al., 2007; Cheon et al., 2015]. More importantly, the seasonality of the Antarctic sea-ice trend in the Atlantic is almost perfectly opposite to that in the East Pacific (Figures 4a and b). The upper ocean temperatures became colder (up to -0.6°C) over the outer edge of sea-ice in the warm seasons (Figure 7c) consistent with the increasing sea-ice fraction (Figure 7a). Similar to the East Pacific, a large warming occurred below the surface (up to 0.7°C) north of 65°S. However, it appears that the subsurface warming has little impact on the upper ocean temperatures during the warm seasons, in contrast to the East Pacific.

As shown in Figure 6a, the SH westerlies increased south of around 50°S over the Atlantic during the warm seasons due to the strengthening of the SH subpolar low over the Antarctic Peninsula and SH subtropical high over the Atlantic. Due to this poleward intensification of the SH westerlies in the Atlantic [e.g., Lee and Feldstein, 2013; Thompson and Solomon, 2002], the northward velocity in the upper 100 m increased during the warm seasons (Figure 8b), which coincides with the cooler upper ocean temperatures and the increasing sea-ice fraction north of 65°S over the outer edge (Figures 7a and c). However, the northward velocity in the upper 100 m did not increase south of 65°S, and thus could not explain the cooler upper ocean temperatures or the increased sea-ice fraction south of 65°S over the outer edge. Figure 8c shows that the seasonal surface warming during November - January tends to weaken, thus reinforcing the increasing sea-ice trend in the outer edge. This positive feedback could explain the large surface cooling trend south of 68°S during the warm seasons (Figure 7c). However, it is unlikely that the positive feedback involving sea-ice, air-sea heat flux and surface ocean temperature is what caused the increasing Antarctic sea-ice fraction in the Weddell Sea during the warm seasons.

During the cold seasons, the upper ocean temperatures in the outer edge of sea-ice are much warmer (up to 0.7°C) especially north of 60°S (Figure 7d) in line with the decreasing sea-ice fraction (Figure 7b). As shown in Figures 6b and 8b, the SH westerlies over the Atlantic weakened considerably during the cold seasons due to the weakening SH subpolar low over the Atlantic-Indian sector, which could be traced back to deep tropical convections in the tropical Atlantic [Simpkins et al., 2014; Lee et al., 2013] and Indian summer monsoon regions [Lee et al., 2013]. The weakening SH westerlies in the Atlantic sharply reduced the northward Ekman transport, which in turn resulted in an anomalous southward Ekman transport of warmer surface water. In addition, the seasonal surface cooling and vertical mixing in the cold seasons could entrain the warmer upper CDW to increase the mixed layer temperatures in the outer edge of sea-ice. Therefore, it is likely that both the anomalous southward Ekman transport of warm surface water and the vertical mixing with the warm upper CDW contributed to the retreat of sea-ice extent in the cold seasons over the Atlantic. Figure 8c shows that the air-sea heat flux over the outer edge of sea-ice tends to suppress the sea-ice trends (i.e., a negative feedback) during the months of climatological surface cooling in March - August. However, the air-sea heat flux immediately north of the outer edge of sea-ice tends to increase in May - July. Due to the seasonal expansion of the sea-ice during these months, the surface warming tendency north of the outer edge could precondition the upper ocean temperatures and thus contribute to the melting sea-ice in the outer edge in austral winter (June - August).

It is clear that Ekman dynamics and air-sea heat flux are not sufficient to explain the seasonality of the Antarctic sea-ice trend in the Atlantic, particularly the increasing sea-ice fraction in the Weddell Sea during the warm seasons. Although other mechanisms such as sea-ice transport and cold- and warm-air advections could potentially contribute, there could be an alternative way that ocean thermal or dynamic processes could affect the seasonality of Antarctic sea-ice trend in the Atlantic. Unlike the East Pacific, the ocean temperature changes in the Atlantic are not limited to the upper few hundred meters, but extend down to 2000 m or even deeper (Figures 7c and d). The ocean temperatures in the upper 2000 m over the Atlantic decreased south of 65°S ~ 58°S and increased north of 65°S ~ 58°S, producing a sharp anomalous meridional thermal gradient in between. Constrained by the thermal wind relationship, the northern branch of the Weddell Gyre strengthened across the increased meridional thermal gradient between 65°S and 55°S (Figures 7e and f). The large increases in the eastward-flowing branch of the Weddell Gyre and the associated meridional thermal gradient indicate that the Weddell Sea is in a geostrophic equilibrium with the poleward intensification of the SH westerlies in the region (Figures 6a and b) [e.g., Lee and Feldstein, 2013; Thompson and Solomon, 2002]. Therefore, we hypothesize that the strengthening northern branch of the Weddell Gyre and the associated increase in the meridional thermal gradient led to the cooler ocean temperatures within the Weddell gyre (i.e., the cold water column pushed toward the north) and the warmer ocean temperatures north of the

Weddell Gyre (i.e., the warm water column pushed toward the south). This hypothesis is consistent with the expansion of sea-ice south of 60°S in the warm seasons and the retreat north of 65°S in the cold seasons (Figures 7a and b).

6. Interannual Variability of West Antarctic Sea-Ice

Our analysis indicates that the increasing SH westerlies in the East Pacific and the poleward strengthening of the SH westerlies in the Atlantic, aided by a positive feedback involving sea-ice, air-sea heat flux and surface ocean temperature, contributed to the seasonally and spatially inhomogeneous sea-ice trends around West Antarctica during the past decades. It should be noted that the long-term trends of the SH westerlies to a certain extent are residuals of local and remotely forced atmospheric modes of variability from synoptic to interannual time scales, such as the SAM, the Pacific-South American patterns [Mo and Higgins, 1998; Lau et al., 1994; Ghil and Mo, 1991] and ENSO-forced extratropical Rossby waves. In particular, the SAM is largely intrinsic atmospheric variability with e-folding time (or de-correlation time) of up to 20 days in the warm seasons and less than 10 days in the cold seasons below the tropopause [e.g., Baldwin et al., 2003]. This suggests a possibility that the long-term trends in Antarctic sea-ice extent are the footprint of decadal changes in the frequency and amplitude of interannual Antarctic sea-ice variability.

Figures 9a and b show the leading EOF modes of detrended Antarctic sea-ice variability for the warm and cold seasons, respectively, derived from the observations. The leading EOF modes show a contrasting pattern of spatial and seasonal sea-ice variations around West Antarctica, which is surprisingly similar to the spatiotemporal pattern of the linear trends (see Figures 1a and b). Interestingly, the leading EOF modes of detrended sea-ice variability around East Antarctica are much weaker. The leading EOF modes derived from the control simulation (Figures 9c and d) are quite consistent with those from the observations. The principal components (PCs) of the leading EOF modes are also highly correlated between the observations and the control simulation (Figures 9e and f).

The apparent similarity between the leading modes of detrended Antarctic sea-ice variability and the linear trends indeed suggests that the linear trends in West Antarctic sea-ice fraction are the residuals of interannual variability in West Antarctic sea-ice driven by similar wind-driven ocean thermal and dynamic processes. However, the leading EOF modes explain only about 20% of the total variance (Figures 9e and f). Therefore, higher EOF modes should be investigated together with the leading modes to better understand the interannual variability of West Antarctic sea-ice and the role of wind-driven ocean thermal and dynamic processes versus other potentially important mechanisms identified in previous studies. Such an in-depth analysis of interannual variability in West Antarctic sea-ice is a subject of future study.

7. Summary and Discussion

We present the potential role of wind-driven ocean thermal and dynamic processes in the spatially and seasonally inhomogeneous sea-ice trends around West Antarctica during the recent decades, using a surface-forced ocean and sea-ice coupled model that reasonably reproduces the observed sea-ice trends around West Antarctica. Our analysis of the model simulation shows that wind-driven ocean thermal and dynamic processes played a crucial role in the summer-fall retreat and winter-spring expansion of Antarctic sea-ice extent in the East Pacific (150°W -

60°W) during the recent decades. As summarized in Figure 10a, the enhanced Ekman upwelling of the warm upper CDW followed by vertical mixing directly contributed to the summer-fall retreat of Antarctic sea-ice extent in the East Pacific over the Amundsen and Bellingshausen Seas, while the increased northward Ekman transport of cold Antarctic surface water contributed to the winter-spring expansion. Both the enhanced upwelling and northward transport were driven by the increasing SH westerlies over the East Pacific.

The linear trends of Antarctic sea-ice in the Atlantic (60°W - 0°) are also strongly affected by wind-driven ocean thermal and dynamic processes. Ekman dynamics still played an active role in the Atlantic particularly in the retreat of sea-ice during the cold seasons. However, the way in which wind-driven ocean dynamics affected the sea-ice trend is quite different and unique in this region. As summarized in Figure 10b, the poleward intensification of SH westerlies in the Atlantic strengthened the eastward-flowing northern branch of the Weddell Gyre. Constrained by the thermal wind relationship, the meridional thermal gradient increased sharply across the northern branch of the Weddell Gyre, cooling the water column within the Weddell Gyre (i.e., the cold water column pushed toward the north) and warming the water column to the north of the Weddell Gyre (i.e., the warm water column pushed toward the south). The colder ocean temperatures within the Weddell Gyre could therefore lead to the expansion of sea-ice extent in the warm seasons, while the warmer ocean temperatures north of the Weddell Gyre could lead to the retreat in the cold seasons.

Although not shown in this study, we have performed an additional CESM1 simulation using the European Centre for Medium-Range Weather Forecasts - Interim (ERA-Interim) surface flux fields [Dee et al., 2011], and another ocean and sea-ice coupled model simulation using the Modular Ocean Model version 5 [Griffies, 2012] with the ERA-Interim surface flux fields. These two additional simulations with different sets of models and surface flux fields provided results that are quite consistent with those presented in this study (not shown), indicating that our conclusions are not restricted to our particular choice of model and surface flux fields. Nevertheless, it is important to point out some of the important limitations in this study. In particular, as discussed in section 2, a constant value of freshwater flux was uniformly distributed along the Antarctic coast in the model simulations. However, recent studies showed that approximately half of the melting water comes from small, warm-cavity ice shelves in the East Pacific occupying only a small fraction of the total Antarctic ice-shelf area [e.g., Rignot et al, 2013]. Additionally, the global sea surface salinity fields, including those in the Antarctic seas, were slowly relaxed to the monthly climatological fields to prevent the model salinity fields from drifting away from the observed climatology. Such treatments of the freshwater discharge and sea surface salinity fields could limit the model's ability to simulate the increasing salinity stratification in the Antarctic seas and its impact on Antarctic sea-ice. It is quite possible that the model's inability to simulate the large Antarctic sea-ice gain in the West Pacific is linked to this limitation in the CESM1 control simulation.

The main conclusion of this study is that the strengthening SH westerlies in the East Pacific and the poleward intensifying SH westerlies in the Atlantic contributed to the inhomogeneity of sea-ice trends around West Antarctica during the past decades via wind-driven ocean thermal and dynamic processes. Given that the observed changes in the SH westerlies over the East Pacific and Atlantic are linked to both the anthropogenic forcing (i.e., the positive trend of SAM due to ozone depletion and increasing greenhouse gases) [e.g., Lee and Feldstein, 2013; Son et al., 2008; Shindell and Schmidt, 2004; Gillett and Thompson, 2003] and natural variability (i.e., induced by the phase changes in the IPO and AMO) [e.g., Lopez et al., 2016; Meehl et al., 2016; Purich et al., 2016; Zhang et al., 2016; Simpkins et al., 2014; Lee et al., 2013], we cannot conclude whether the observed Antarctic sea-ice trends are of anthropogenic origin or due to natural variability.

The results of this study leave open some important scientific questions, which deserve future investigation. Most importantly, the wind-driven ocean thermal and dynamic processes identified in this study should work in concert with various other mechanisms identified in earlier studies, particularly wind-driven sea-ice transport [Holland and Kwok, 2012] and cold- and warm-air advections linked to IPO, AMO and SAM [Purich et al., 2016; Meehl et al. 2016; Clem and Renwick, 2015; Li et al., 2014] and warming-induced surface freshening [e.g., Bintanja et al., 2015; de Lavergne et al., 2014; Bintanja et al., 2013; Zhang, 2007]. A more consistent and thorough mechanism will emerge when all the key factors and their interactions are considered together. For example, our analysis suggests that there exists a positive feedback involving sea-ice, air-sea heat flux and surface ocean temperature during the months of seasonal surface warming in November - January in both the East Pacific and Atlantic. Such positive feedback will amplify Antarctic sea-ice loss or gain in the warm seasons regardless of the triggering mechanism.

Finally, the new findings reported in this study support the ongoing international efforts to implement a sustained in-situ ocean observation system in the Southern Ocean including the

Antarctic seas [Russell et al., 2014; Rintoul et al., 2012]. Since standard Argo floats are hindered from transmitting data under sea-ice, alternative observation platforms suitable for sub-ice ocean profile measurement, such as ice-tethered profilers, underwater gliders and polar profiling floats [Abrahamsen, 2014] are being tested and used to augment the existing ocean observation systems such as the repeated high-density Expendable Bathythermographs (XBT) transects along AX22, AX25, and IX28. Establishing a sustained in-situ ocean observation system in the Antarctic seas will increase our ability to better monitor and predict future changes in Antarctic sea-ice and their far reaching impacts on the global thermohaline ocean circulation [e.g., Abernathey et al., 2016], deep water formation and warming in the Southern Ocean [e.g., Cheon et al., 2015; de Lavergne et al., 2014; Gordon, 2014], the global carbon cycles [e.g., Rysgaard et al., 2011], and the Antarctic marine ecosystem [e.g., Brierley et al., 2002].

Acknowledgments

The Hadley Center sea-ice and SST data set were provided by UK Met Office at http://www.metoffice.gov.uk/hadobs/hadisst, 20CR and MERRA surface flux data sets were, respectively, provided by NOAA/ESRL/PSD at http://www.esrl.noaa.gov/psd, and by NASA/GSFC/GMAO at http://gmao.gsfc.nasa.gov/reanalysis/MERRA. We would like to thank Greg Foltz for helpful comments and suggestions. S.-K. Lee acknowledges Steven Yeager for useful discussions on the CESM1 model simulations, and Libby Johns for proofreading the manuscript. This work was supported by NOAA Atlantic Oceanographic and Meteorological Laboratory. A. L. Gordon acknowledges support provided under the CICAR award number NA08OAR4320754 from NOAA. Lamont-Doherty Earth Observatory contribution number xxxx.

References

Abernathey, R. P., I. Cerovecki, P. R. Holland, E. Newsom, M. Mazloff, and L. D. Talley (2016), Water-mass transformation by sea ice in the upper branch of the Southern Ocean overturning, *Nat. Geosci.*, doi:10.1038/ngeo2749.

Abrahamsen, E. P. (2014), Sustaining observations in the polar oceans, *Philos. Trans. Roy. Soc. London Ser. A*, *372*, 20130337, doi:10.1098/rsta.2013.0337.

Baldwin, M. P., D. B. Stephenson, D. W. Thompson, T. J. Dunkerton, A. J. Charlton, and A. O'Neill (2003), Stratospheric memory and skill of extended-range weather forecasts. *Science*, *301*, 636-640.

Bintanja, R., G. J. Van Oldenborgh, S. S. Drijfhout, B. Wouters, and C. A. Katsman (2013), Important role for ocean warming and increased ice-shelf melt in Antarctic sea-ice expansion, *Nat. Geosci.*, *6*, 376-379.

Bintanja, R., G. J. Van Oldenborgh, and C. A. Katsman (2015), The effect of increased fresh water from Antarctic ice shelves on future trends in Antarctic sea ice, *Ann. Glaciol.*, *56*, 120-126.

Brierley, A. S., P. G. Fernandes, M. A. Brandon, F. Armstrong, N. W. Millard, S. D. McPhail, P. Stevenson, M. Pebody, J. Perrett, M. Squires, D. G. Bone (2002), Antarctic krill under sea ice: elevated abundance in a narrow band just south of ice edge, *Science*, *295*, 1890-1892.

Cheon, W. G., S.-K. Lee, A. L. Gordon, Y. Liu, C.-B. Cho and J. Park (2015), Replicating the 1970s' Weddell Polynya using a coupled ocean - sea ice model with reanalysis surface flux fields, *Geophys. Res. Lett.*, *42*, 5411-5418, doi:10.1002/2015GL064364.

Clem, K. R., and J. A. Renwick (2015), Austral spring Southern Hemisphere circulation and temperature changes and links to the SPCZ, *J. Clim.*, *28*, 7371-7384.

Compo, G. P., J. S. Whitaker, P. D. Sardeshmukh, N. Matsui, R. J. Allan, X. Yin, B. E. Gleason R.S. Vose, G. Rutledge, P. Bessemoulin, and S. Brönnimann (2011), The twentieth century reanalysis project, *Q. J. R. Meteorol. Soc.*, *137*, 1–28.

Danabasoglu, G., S. C. Bates, B. P. Briegleb, S. R. Jayne, M. Jochum, W. G. Large, S. Peacock, and S. G. Yeager (2012), The CCSM4 ocean component, *J. Clim.*, *25*, 1361–1389.

Dai, A. and K. E. Trenberth (2002), Estimates of freshwater discharge from continents: Latitudinal and seasonal variations, *J. Hydrometeorol.*, *3*, 660-687.

Dee, D. P., S. M. Uppala, A. J. Simmons, P. Berrisford, P. Poli, S. Kobayashi, U. Andrae, M. A. Balmaseda, G. Balsamo, P. Bauer, and P. Bechtold (2011), The ERA-Interim reanalysis: Configuration and performance of the data assimilation system, *Q. J. R. Meteorol. Soc.*, 137, 553-597.

de Lavergne, C., J. B. Palter, E. D. Galbraith, R. Bernardello, and I. Marinova (2014), Cessation of deep convection in the open Southern Ocean under anthropogenic climate change, *Nat. Clim. Change*, *4*, 278–282.

Ding, Q., E. J. Steig, D. S. Battisti, and M. Küttel (2011), Winter warming in West Antarctica caused by central tropical Pacific warming, *Nat. Geosci.*, *4*, 398-403.

Ebert, E. E., and J. A. Curry (1993), An intermediate one-dimensional thermodynamic sea ice model for investigating ice-atmosphere interactions, *J. Geophys. Res.*, *98*, 10,085 – 10,109.

Enfield, D. B., A. M. Mestas-Nuñez, and P. J. Trimble (2001), The Atlantic multidecadal oscillation and its relation to rainfall and river flows in the continental US., *Geophys. Res. Lett.*, *28*, 2077-2080.

Gent, P. R., and G. Danabasoglu (2011), Response to increasing Southern Hemisphere winds in CCSM4, *J. Clim., 24*, 4992–4998.

Ghil, M., and K. C. Mo (1991), Intraseasonal oscillations in the global atmosphere. Part II: Southern Hemisphere. *J. Atmos. Sci*., *48*, 780–790.

Gillett, N. P., and D. W. J. Thompson (2003), Simulation of recent Southern Hemisphere climate change, *Science*, *302*, 273-275.

Gordon, A. L., and H. W. Taylor (1975), Seasonal change of Antarctic Sea ice cover. *Science*, *187*, 346-347.

Gordon, A. L., M. Visbeck, and J. C. Comiso (2007), A possible link between the Weddell Polynya and the Southern Annular Mode, *J. Clim*., *20*, 2558–2571.

Gordon, A. L. (2014), Oceanography: Southern Ocean polynya, *Nat. Clim. Change*, *4*, 249-250.

Griffies, S. M. (2012), Elements of the modular ocean model (MOM), NOAA/Geophysical Fluid Dynamics Laboratory, Princeton, NJ, 632 pp.

Holland, P. R., and R. Kwok (2012), Wind-driven trends in Antarctic sea-ice drift. *Nat. Geosci.*, *5*, 872-875.

Hunke, E. C., and W. H. Lipscomb (2008), CICE: The Los Alamos Sea Ice Model, documentation and software, version 4.0. Los Alamos National Laboratory Tech. Rep. LA-CC-06-012, 76pp.

Jacobs, S. S., H. Hellmer, C. Doake, and R. Frolich (1992), Melting of ice shelves and the mass balance of Antarctica, *J. Glaciol*., *38*, 375–387.

Ji, X., J. D. Neelin, S.-K. Lee, and C. R. Mechoso (2014), Interhemispheric teleconnections from tropical heat sources in intermediate and simple models, *J. Clim*., *27*, 684-697.

Kirtman, B. P., C. M. Bitz, F. Bryan, W. Collins, J. Dennis, N. Hearn, J. L. Kinter III, R. Loft, C. Rousset, L. Siqueira, and C. Stan (2012), Impact of ocean model resolution on CCSM climate simulations, *Clim. Dyn*., *39*, 1303 - 1328.

Kwok, R., and J. C. Comiso (2002), Southern Ocean climate and sea ice anomalies associated with the Southern Oscillation, *J. Clim.*, *15*, 487-501.

Landrum, L., M. M. Holland, D. P. Schneider, E. Hunke (2012), Antarctic sea ice climatology, variability, and late twentieth-century change in CCSM4, *J. Clim.*, *25*, 4817-4838.

Large, W. G., and S. G. Yeager (2009), The global climatology of an interannually varying air–sea flux data set, *Clim. Dyn., 33*, 341–364.

Lau, M. K., P. J. Sheu, and I. S. Kang (1994), Multiscale low-frequency circulation modes in the global atmosphere, *J. Atmos. Sci*., *51*, 2753–2750.

Lee, S. and S. B. Feldstein (2013), Detecting ozone-and greenhouse gas–driven wind trends with observational data, *Science*, *339*, 563-567.

Lee, S.-K., C. R. Mechoso, C. Wang, and J. D. Neelin (2013), Interhemispheric influence of the northern summer monsoons on the southern subtropical anticyclones. *J. Clim.*, *26*, 10193-10204.

Lee, S.-K., W. Park, E. van Sebille, M. O. Baringer, C. Wang, D. B. Enfield, S. Yeager and B. P. Kirtman (2011), What caused the significant increase in Atlantic ocean heat content since the mid-20th century?, *Geophys. Res. Lett*., *38*, L17607, doi:10.1029/2011GL048856

Lee, S.-K., W. Park, M. O. Baringer, A. L. Gordon, B. Huber and Y. Liu (2015), Pacific origin of the abrupt increase in Indian Ocean heat content during the warming hiatus, *Nat. Geosci.*, *8*, 445-449, doi:10.1038/ngeo2438.

Legler, D. M., H. J. Freeland, R. Lumpkin, G. Ball, M. J. McPhaden, S. North, R. Crowley, G. J. Goni, U. Send and M. A. Merrifield (2015), The current status of the real-time in situ global ocean observing system for operational oceanography, *J. Oper. Oceanogr*, *8*, sup2, s189-s200.

Li, X., D. M. Holland, E. P. Gerber, and C. Yoo (2014), Impacts of the north and tropical Atlantic Ocean on the Antarctic Peninsula and sea ice, *Nature*, *505*, 538-542.

Liu, J., J. A. Curry, and D. G. Martinson (2004), Interpretation of recent Antarctic sea ice variability, *Geophys. Res. Lett.*, *31*, L02205, doi:10.1029/2003GL018732.

Liu, Y., S.-K. Lee, D. B. Enfield, B. A. Muhling, J. T. Lamkin, F. Muller-Karger and M. A. Roffer (2015), Potential impact of climate change on the Intra-Americas Seas: Part-1. A dynamic downscaling of the CMIP5 model projections. *J. Marine Syst.*, *148*, 56-69, doi:10.1016/j.jmarsys.2015.01.007.

Lopez, H., S. Dong, S.-K. Lee, and E. Campos (2016), Remote influence of Interdecadal Pacific Oscillation on the South Atlantic meridional overturning circulation variability, *Geophys. Res. Lett.*, *43*, 8250–8258, doi:10.1002/2016GL069067.

Matear, R. J., T. J. O'Kane, J. S. Risbey, and M. Chamberlain (2015), Sources of heterogeneous variability and trends in Antarctic sea-ice. *Nat. Commun.*, *6*, 8656.

Meehl, G. A., J. M. Arblaster, J. Y. Fasullo, A.Hu, and K. E. Trenberth (2011), Model-based evidence of deep ocean heat uptake during surface temperature hiatus periods, *Nat. Clim. Change, 1*, 360 – 364.

Meehl, G. A., J. M. Arblaster, C. M. Bitz, C. T. Chung, and H. Teng (2016), Antarctic sea-ice expansion between 2000 and 2014 driven by tropical Pacific decadal climate variability, *Nat. Geosci.*, doi:10.1038/ngeo2751.

Meyer, B., A. Atkinson, B. Blume, and U. V. Bathmann (2002), Feeding and energy budgets of Antarctic krill Euphausia superba at the onset of winter–I–Furcilia III larvae, *Limnol. Oceanogr.*, *47*, 943–952.

Mo, K. C., and R. W. Higgins (1998), The Pacific-South American modes and tropical convection during the Southern Hemisphere winter, *Mon. Weather Rev.*, *126*, 1581-1596.

Parkinson, C. L., and D. J. Cavalieri (2012), Antarctic sea ice variability and trends, 1979–2010, *Cryosphere*, *6*, 871-880, doi:10.5194/tc-6-871-2012, 2012.

Piñones, A. and A. V. Fedorov (2016), Projected changes of Antarctic krill habitat by the end of the 21st century, *Geophys. Res. Lett.*, *43*, doi:10.1002/2016GL069656.

Purich, A., M. H. England, W. Cai, Y. Chikamoto, A. Timmermann, J. C. Fyfe, L. Frankcombe, G. A. Meehl, and J. M. Arblaster (2016), Tropical Pacific SST drivers of recent Antarctic sea ice trends, *J. Clim.*, doi:10.1175/JCLI-D-16-0440.1, in press.

Rayner, N. A., D. E. Parker, E. B. Horton, C. K. Folland, L. V. Alexander, D. P. Rowell, E. C. Kent, and A. Kaplan (2003), Global analyses of sea surface temperature, sea ice, and night marine air temperature since the late nineteenth century, *J. Geophys. Res.*, *108*, 4407, doi:10.1029/2002JD002670, D14.

Renwick, J. A. (2002), Southern Hemisphere circulation and relations with sea ice and sea surface temperature, *J. Clim.*, *15*, 3058-3068.

Rienecker, M. M. et al. (2011), MERRA: NASA's Modern-Era Retrospective analysis for Research and Applications, *J. Clim.*, *24*, 3624-3648, doi:10.1175/JCLI-D-11-00015.1.

Rignot, E., S. Jacobs, J. Mouginot, and B. Scheuchl (2013), Ice-shelf melting around Antarctica, *Science*, *341*, 266-270.

Rintoul, S. R., M. Sparrow, M. P. Meredith, V. Wadley, K. Speer, E. Hofmann, C. P. Summerhayes, E. Urban, R. Bellerby, S. Ackley, and K. Alverson (2012), The Southern Ocean observing system: initial science and implementation strategy, Cambridge, UK: Scientific Committee on Antarctic Research, 74 pp.

Russell, J. R., J. L. Sarmiento, H. Cullen, R. Hotinski, K. Johnson, S. Riser, and L. Talley (2014), The Southern Ocean Carbon and Climate Observations and Modeling Program (SOCCOM), *Ocean Carbon and Biogeochemistry Newsletter*, *7*, 1-5.

Rysgaard, S., J. Bendtsen, B. Delille, G. S. Dieckmann, R. N. Glud, H. Kennedy, J. Mortensen, S. Papadimitriou, D. N. Thomas, and J.-L. Tison (2011), Sea ice contribution to the air-sea CO_2 exchange in the Arctic and Southern Oceans, *Tellus B*, *63*, 823-830.

Shindell, D. T., and G. A. Schmidt (2004), Southern Hemisphere climate response to ozone changes and greenhouse gas increases, *Geophys. Res. Lett.*, *31*, L18209, doi:10.1029/2004GL020724.

Simpkins, G. R., S. McGregor, A. S. Taschetto, L. M. Ciasto, M. H. England (2014), Tropical connections to climatic change in the extratropical Southern Hemisphere: The role of Atlantic SST trends, *J. Clim.*, *27*, 4923-4936.

Son, S.-W., L. M. Polvani, D. W. Waugh, H. Akiyoshi, R. R. Garcia, D. Kinnison, S. Pawson, E. Rozanov, T. G. Shepherd, and K. Shibata (2008), The impact of stratospheric ozone recovery on the Southern Hemisphere westerly jet, *Science*, *320*, 1486–1489.

Stammerjohn, S. E., D. G. Martinson, R. C. Smith, X. Yuan, D. and Rind (2008), Trends in Antarctic annual sea ice retreat and advance and their relation to El Niño–Southern Oscillation and Southern Annular Mode variability, *J. Geophys. Res.*, *113*, C03S90, doi:10.1029/2007JC004269.

Steele, M., R. Morley, and W. Ermold (2001), A global ocean hydrography with a high-quality Arctic Ocean, *J. Clim*., *14*, 2079–2087.

Stroeve, J. C., V. Kattsov, A. Barrett, M. Serreze, T. Pavlova, M. Holland, and W. N. Meier (2012), Trends in Arctic sea ice extent from CMIP5, CMIP3 and observations, *Geophys. Res. Lett*., *39*, L16502, doi:10.1029/2012GL052676.

Takahashi, T. et al., , Sutherland, S. C., Wanninkhof, R., Sweeney, C., Feely, R. A., Chipman, D. W., Hales, B., Friederich, G., Chavez, F., Sabine, C., Watson, A., Bakker, D. C. E., Schuster, U., Metzl, N., Inoue, H. Y., Ishii, M., Midorikawa, T., Nojiri, Y., Ko- ertzinger, A., Steinhoff, T., Hoppema, M., Olafsson, J., Arnar- son, T. S., Tilbrook, B., Johannessen, T., Olsen, A., Bellerby, R., Wong, C. S., Delille, B., Bates, N. R., and de Baar, H. J. W.: Climatological mean and decadal change in surface ocean pCO_2, and net sea-air CO_2 flux over the global oceans, *Deep-Sea Res. II*, *56*, 554–577, doi:10.1016/j.dsr2.2008.12.009, 2009.

Talley L. D., G. L. Pickard, W. J. Emery, J. H. Swift (2011), Descriptive physical oceanography: An introduction (Sixth Edition), Elsevier, Boston, 560 pp.

Thompson, D. W. J., and S. Solomon (2002), Interpretation of recent Southern Hemisphere climate change, *Science*, 296, 895-899.

Turner, J., and J. Overland (2009), Contrasting climate change in the two polar regions, *Polar Res.*, *28*, 146–164.

Walsh, J. E. (1983), The role of sea ice in climatic variability: Theories and evidence, *Atmos.-Ocean*, *21*, 229 - 242.

Wang, C., S.-K. Lee, and C. R. Mechoso (2010), Inter-hemispheric influence of the Atlantic warm pool on the southeastern Pacific, *J. Clim.*, *23*, 404-418.

Wanninkhof, R., G.-H. Park, T. Takahashi, C. Sweeney, R. Feely, Y. Nojiri, N. Gruber, S. C. Doney, G. A. McKinley, A. Lenton, C. Le Quéré, C. Heinze, J. Schwinger, H. Graven and S. Khatiwala (2013), Global ocean carbon uptake: magnitude, variability and trends, *Biogeosciences*, *10*, 1983-2000.

Wu, Y., X. Zhai, X, and Z. Wang (2016), Impact of synoptic atmospheric forcing on the mean ocean circulation, *J. Clim*., *29*, 5709 - 5724.

Yuan, X. (2004), ENSO-related impacts on Antarctic sea ice: a synthesis of phenomenon and mechanisms, *Antarct. Sci*., *16*, 415-25.

Yuan, X., and C. Li (2008), Climate modes in southern high latitudes and their impacts on Antarctic sea ice, *J. Geophys. Res.*, *113*, C06S91, doi:10.1029/2006JC004067.

Zhang, J. (2007), Increasing Antarctic sea ice under warming atmospheric and oceanic conditions, *J. Clim*., *20*, 2515 - 2529.

Zhang, L., T. L. Delworth, and F. Zeng (2016), The impact of multidecadal Atlantic meridional overturning circulation variations on the Southern Ocean, *Clim. Dyn*., doi:10.1007/s00382-016-3190-8.

Figure 1. Linear trends of Antarctic sea-ice fraction during (a,c) the warm (December - May) and (b,d) cold (June - November) seasons, obtained from (a,b) the Hadley Center sea-ice and sea surface temperature data sets over the period of 1979 - 2014 and (c,d) the CESM1 control simulation over the period of 1985 - 2014. The first six years (1979 - 1984) of the model results were excluded to prevent any potential model drift in the beginning of the control simulation from affecting the modeled sea-ice trend. The units are % in 35 years.

Figure 2. The oceans and regional seas around Antarctica. The thick red lines indicate the boundaries of the East Pacific (150°W - 60°W) and Atlantic (60°W - 0°) used in this study.

Figure 3. Linear trends of Antarctic sea-ice fraction averaged in (a,b) the East Pacific (150°W - 60°W) and (c,d) Atlantic (60°W - 0°) for each calendar month, obtained from (a,c) the CESM1 control simulation over the period of 1984 - 2014 and (b,d) the Hadley Center sea-ice and sea surface temperature data sets over the period of 1979 - 2014. The two green lines in each panel represent 5 and 90% climatological sea-ice fractions. The units are % in 35 years.

Figure 4. Linear trends of (a,b) Antarctic sea-ice fraction and (c,d) ocean temperatures averaged in the East Pacific (150°W - 60°W) for (a,c) the warm and (b,d) cold seasons over the period of 1985 - 2014, obtained from the CESM1 control simulation. Linear trends of observed Antarctic sea-ice fraction over the period of 1979 - 2014 averaged in the East Pacific are also shown in (a,b). The black lines in (c,d) indicate the climatological temperatures. The units are % in 35 years for sea-ice fraction and °C in 35 years for ocean temperature.

Figure 5. Linear trends of (a) meridional velocity averaged in the upper 100 m (shades) and zonal wind stress (contours), (b) vertical velocity at 100 m (shades) and wind stress curl (contours), and (c) sea-ice fraction (shades) and net air-sea heat flux (contours) over the period of 1985 - 2014 averaged in the East Pacific (150°W - 60°W) for each of calendar month, obtained from the CESM1 control simulation. These fields are not shown for the inner edge of climatological sea-ice extent (i.e., above 90% sea-ice fraction). The units are 10^{-2} ms^{-1} in 35

years for meridional velocity, 10^{-4} ms^{-1} in 35 years for vertical velocity and 10^{-6} Nm^{-3} in 35 years for wind stress curl, % in 35 years for sea-ice fraction, and Wm^{-2} in 35 years for air-sea heat flux.

Figure 6. Linear trends of sea level pressure (shades) derived from MERRA and surface wind stress vectors (arrows) derived from the CESM1 control simulation over the period of 1985 - 2014 during (a) the warm and (b) cold seasons. The units are hPa in 35 years for sea level pressure, and 10^{-1} Nm^{2} in 35 years for wind stress vectors.

Figure 7. Linear trends of (a,b) Antarctic sea-ice fraction, (c,d) ocean temperatures, and (e,f) zonal velocity averaged in the Atlantic (60°W - 0°) for (a,c,e) the warm and (b,d,e) cold seasons over the period of 1985 - 2014, obtained from the CESM1 control simulation. Linear trends of observed Antarctic sea-ice fraction over the period of 1979 – 2014 averaged in the Atlantic are also shown in (a,b). The black lines in (c,d) and (e,f) indicate the climatological temperatures and zonal velocity, respectively. The units are % in 35 years for sea-ice fraction, °C in 35 years for ocean temperature and cms^{-1} in 35 years for zonal velocity.

Figure 8. As in Figure 5, but for the Atlantic (60°W - 0°).

Figure 9. Leading Empirical Orthogonal Function (EOF) modes of detrended Antarctic sea-ice fraction variability during (a,c) the warm and (b,d) cold seasons, obtained from (a,b) the Hadley Center sea-ice and sea surface temperature data sets over the period of 1979 - 2014 and (c,d) the CESM1 control simulation over the period of 1985 - 2014. The normalized principal components (PCs) of the leading modes are also shown in (e,f). The percentage variance explained by each of

the leading modes, and the correlations between the PCs derived from the observations and the control simulation are indicated in (e,f). The units in (a-d) are % per two units of the normalized PCs.

Figure 10. Sketch of the physical mechanisms linking the wind-driven ocean dynamics and the Antarctic sea-ice trends in (a) the East Pacific and (b) Atlantic. In the East Pacific, the strengthening SH westerlies enhanced Ekman upwelling of the warm upper CDW and increased the northward Ekman transport of cold Antarctic surface water, thus contributing to the expansion of sea-ice in the cold seasons and to the retreat in the warm seasons. In the Atlantic, the poleward intensification of SH westerlies strengthened the northern branch of the Weddell Gyre. Constrained by the thermal wind balance, the meridional thermal gradient increased across the northern branch of the Weddell Gyre, cooling the water column within the Weddell Gyre and warming the water column to the north of the Weddell Gyre, thus contributing to the expansion of sea-ice within the Weddell Gyre in the warm seasons, and to the retreat north of the Weddell Gyre in the cold seasons.

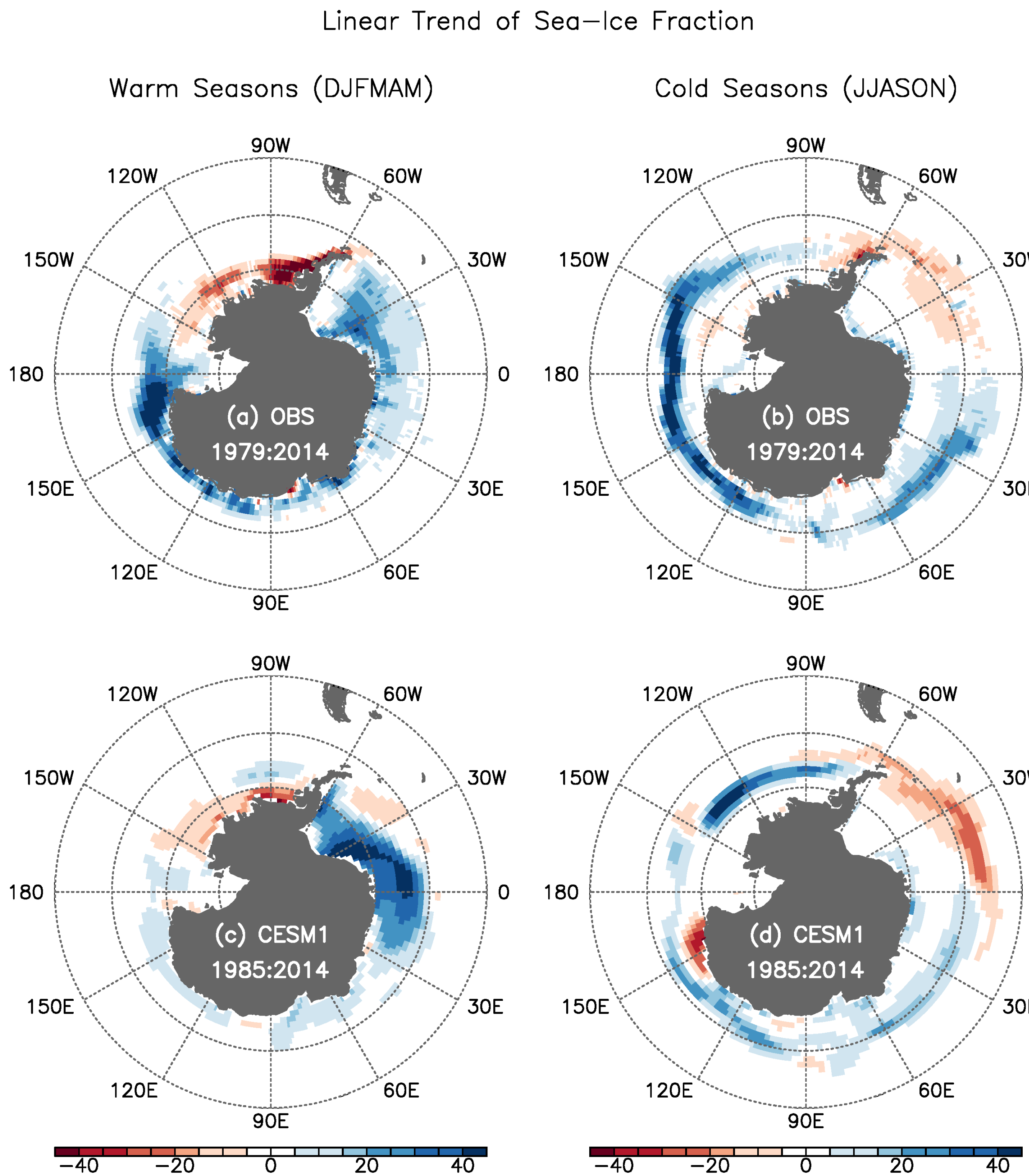

Figure 1. Linear trends of Antarctic sea-ice fraction during (a,c) the warm (December - May) and (b,d) cold (June - November) seasons, obtained from (a,b) the Hadley Center sea-ice and sea surface temperature data sets over the period of 1979 - 2014 and (c,d) the CESM1 control simulation over the period of 1985 - 2014. The first six years (1979 - 1984) of the model results were excluded to prevent any potential model drift in the beginning of the control simulation from affecting the modeled sea-ice trend. The units are % in 35 years.

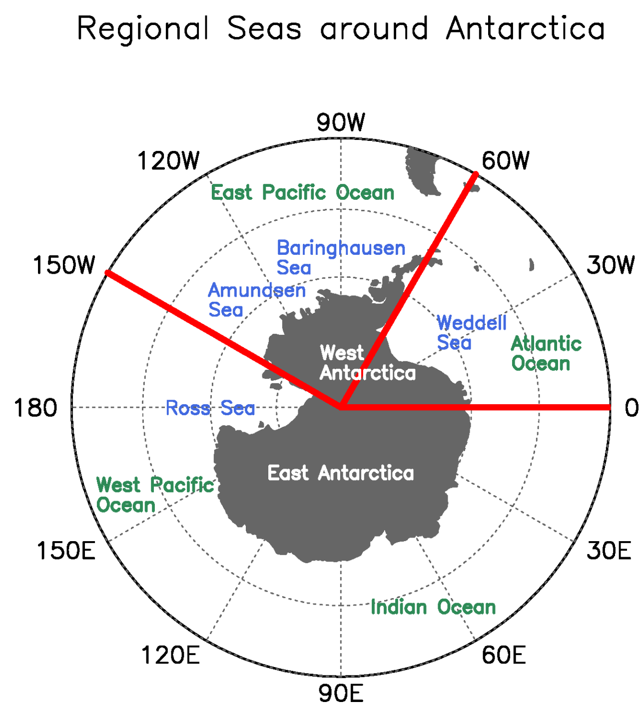

Figure 2. The oceans and regional seas around Antarctica. The thick red lines indicate the boundaries of the East Pacific (150°W - 60°W) and Atlantic (60°W - 0°) used in this study.

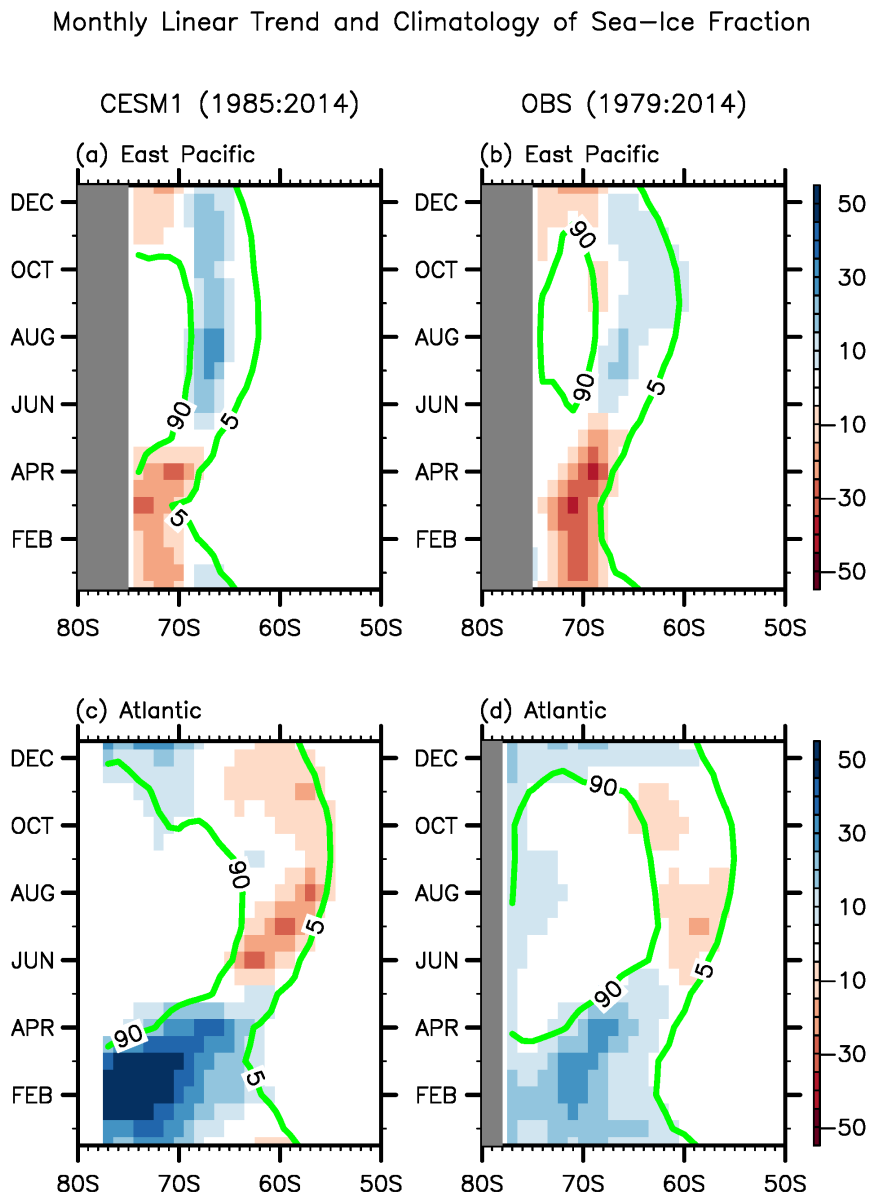

Figure 3. Linear trends of Antarctic sea-ice fraction averaged in (a,b) the East Pacific (150°W - 60°W) and (c,d) Atlantic (60°W - 0°) for each calendar month, obtained from (a,c) the CESM1 control simulation over the period of 1984 - 2014 and (b,d) the Hadley Center sea-ice and sea surface temperature data sets over the period of 1979 - 2014. The two green lines in each panel represent 5 and 90% climatological sea-ice fractions. The units are % in 35 years.

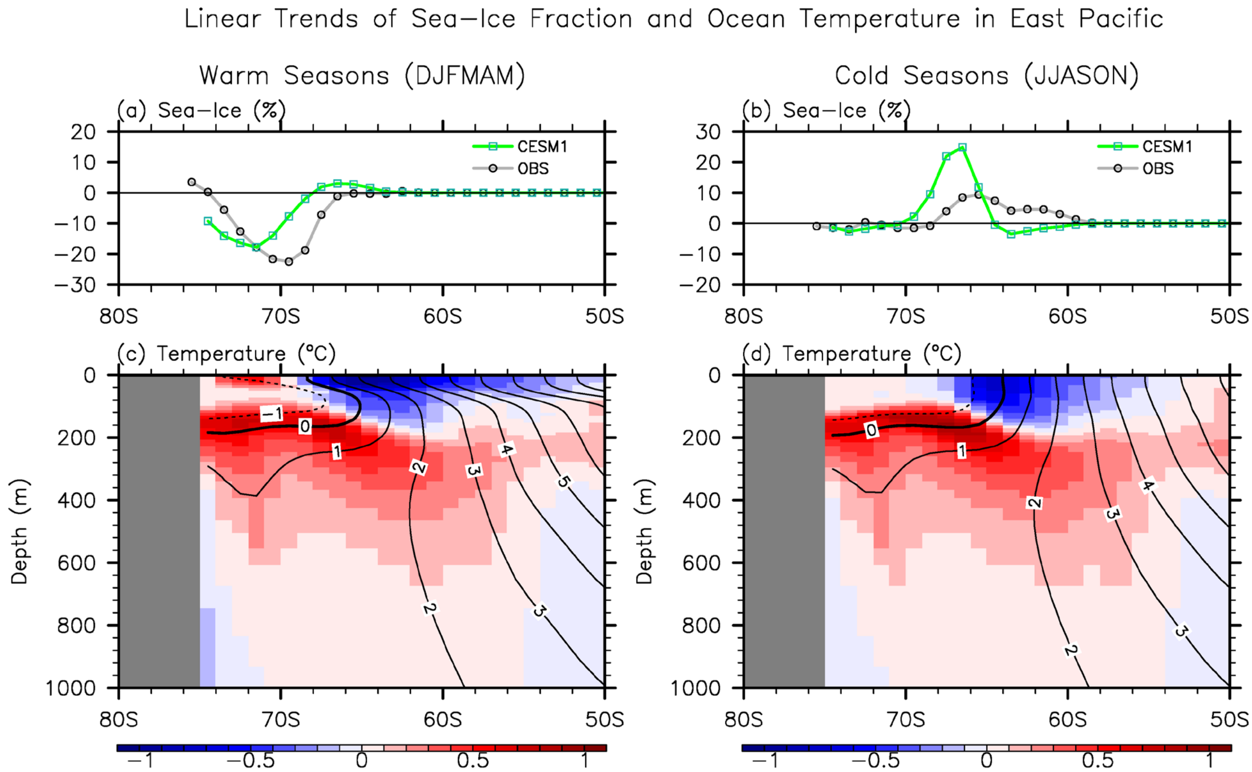

Figure 4. Linear trends of (a,b) Antarctic sea-ice fraction and (c,d) ocean temperatures averaged in the East Pacific (150°W - 60°W) for (a,c) the warm and (b,d) cold seasons over the period of 1985 - 2014, obtained from the CESM1 control simulation. Linear trends of observed Antarctic sea-ice fraction over the period of 1979 - 2014 averaged in the East Pacific are also shown in (a,b). The black lines in (c,d) indicate the climatological temperatures. The units are % in 35 years for sea-ice fraction and °C in 35 years for ocean temperature.

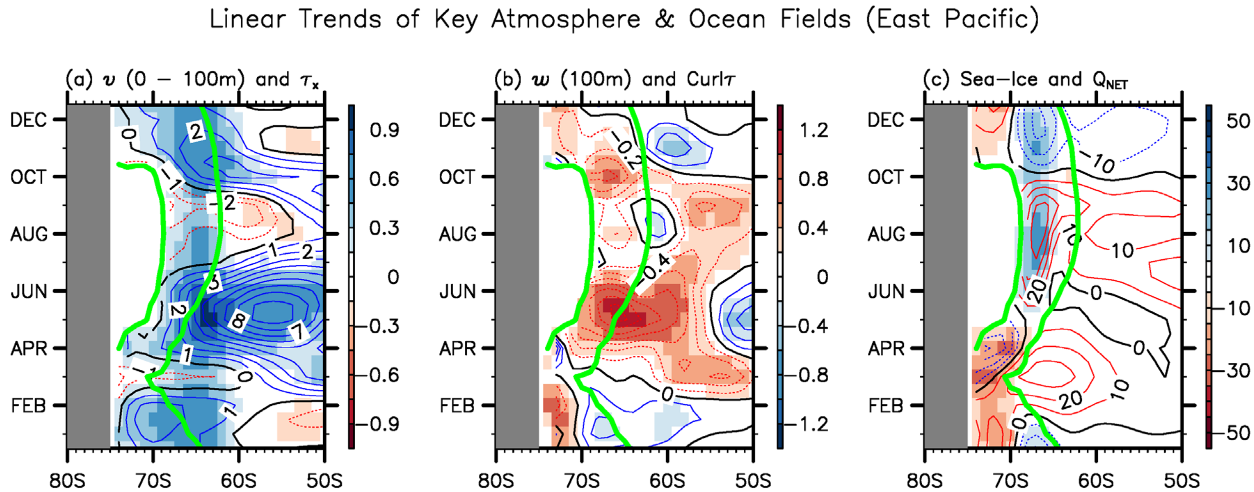

Figure 5. Linear trends of (a) meridional velocity averaged in the upper 100 m (shades) and zonal wind stress (contours), (b) vertical velocity at 100 m (shades) and wind stress curl (contours), and (c) sea-ice fraction (shades) and net air-sea heat flux (contours) over the period of 1985 - 2014 averaged in the East Pacific (150°W - 60°W) for each of calendar month, obtained from the CESM1 control simulation. These fields are not shown for the inner edge of climatological sea-ice extent (i.e., above 90% sea-ice fraction). The units are 10^{-2} ms^{-1} in 35 years for meridional velocity, 10^{-4} ms^{-1} in 35 years for vertical velocity and 10^{-6} Nm^{-3} in 35 years for wind stress curl, % in 35 years for sea-ice fraction, and Wm^{-2} in 35 years for air-sea heat flux.

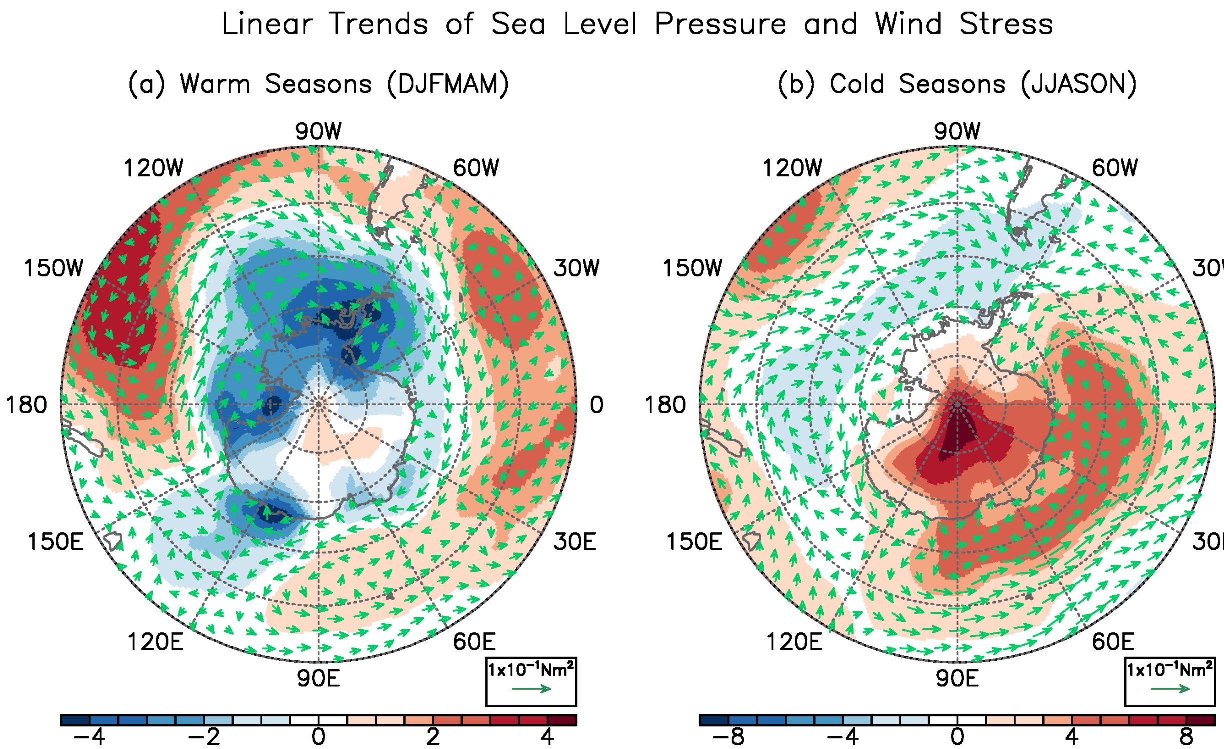

Figure 6. Linear trends of sea level pressure (shades) derived from MERRA and surface wind stress vectors (arrows) derived from the CESM1 control simulation over the period of 1985 - 2014 during (a) the warm and (b) cold seasons. The units are hPa in 35 years for sea level pressure, and 10^{-1} Nm^2 in 35 years for wind stress vectors.

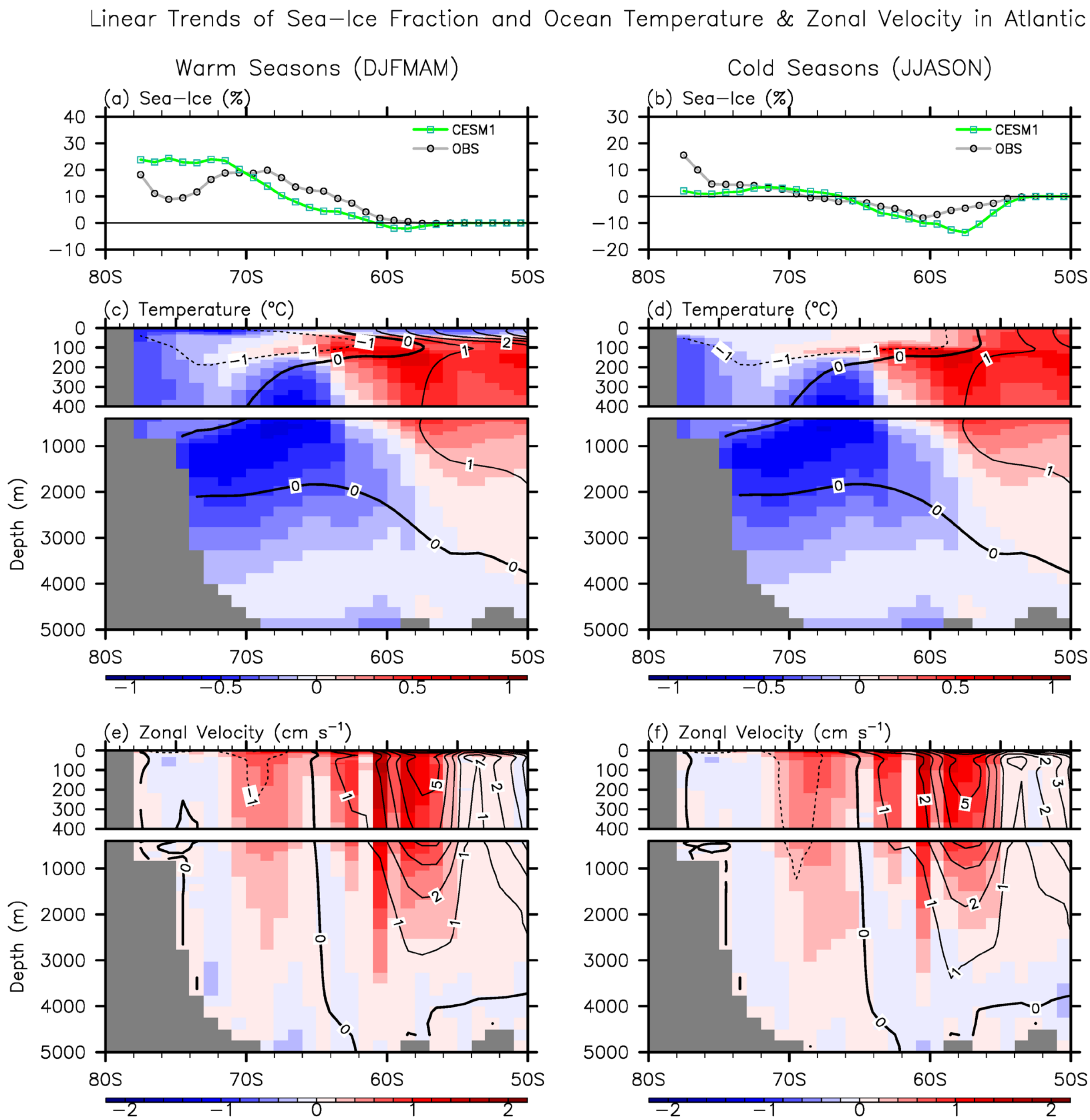

Figure 7. Linear trends of (a,b) Antarctic sea-ice fraction, (c,d) ocean temperatures, and (e,f) zonal velocity averaged in the Atlantic (60°W - 0°) for (a,c,e) the warm and (b,d,e) cold seasons over the period of 1985 - 2014, obtained from the CESM1 control simulation. Linear trends of observed Antarctic sea-ice fraction over the period of 1979 – 2014 averaged in the Atlantic are also shown in (a,b). The black lines in (c,d) and (e,f) indicate the climatological temperatures and zonal velocity, respectively. The units are % in 35 years for sea-ice fraction, °C in 35 years for ocean temperature and cms^{-1} in 35 years for zonal velocity.

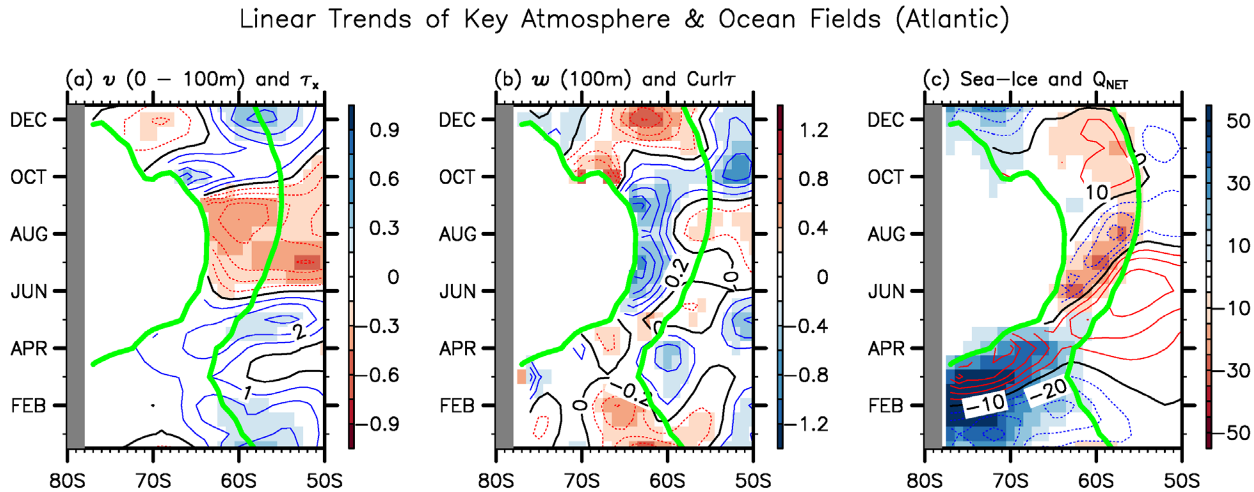

Figure 8. As in Figure 5, but for the Atlantic (60°W - 0°).

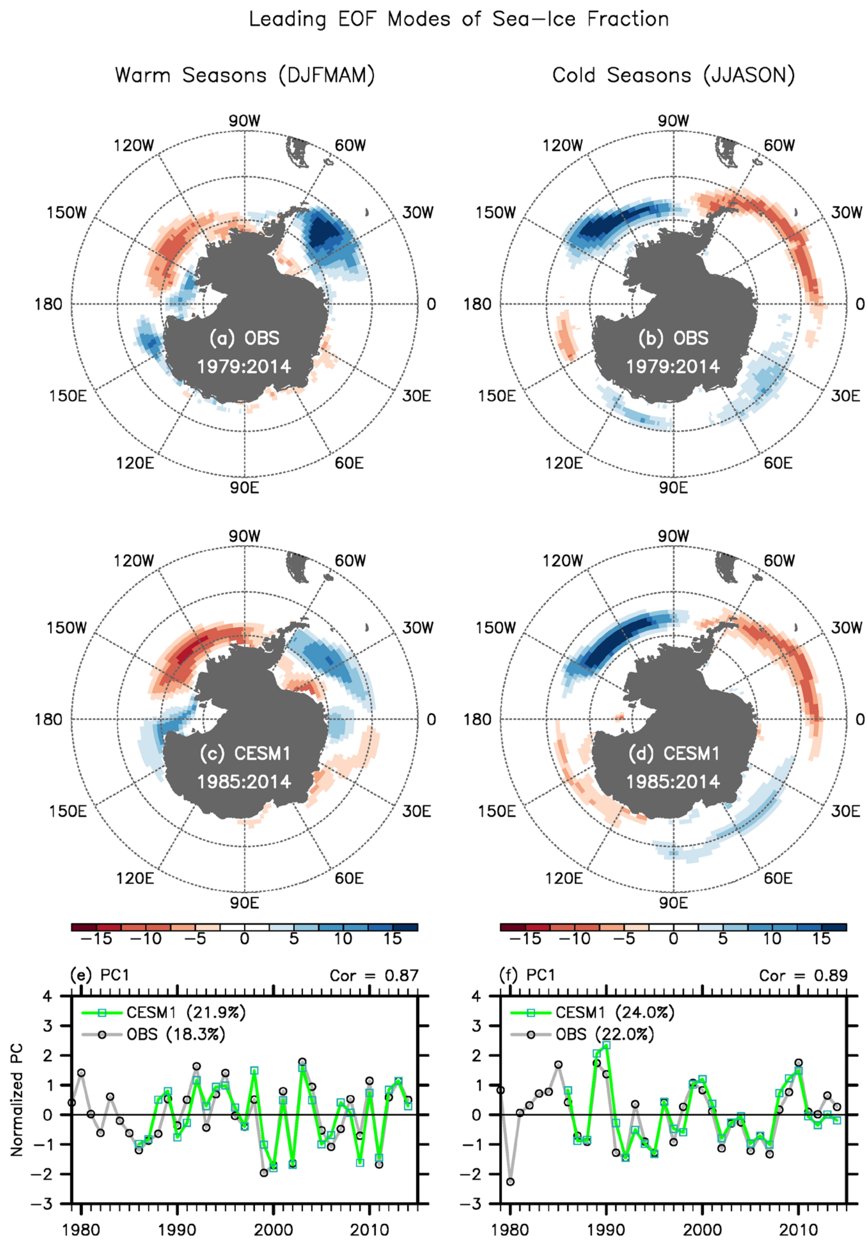

Figure 9. Leading Empirical Orthogonal Function (EOF) modes of detrended Antarctic sea-ice fraction variability during (a,c) the warm and (b,d) cold seasons, obtained from (a,b) the Hadley Center sea-ice and sea surface temperature data sets over the period of 1979 - 2014 and (c,d) the CESM1 control simulation over the period of 1985 - 2014. The normalized principal components (PCs) of the leading modes are also shown in (e,f). The percentage variance explained by each of the leading modes, and the correlations between the PCs derived from the observations and the control simulation are indicated in (e,f). The units in (a-d) are % per two units of the normalized PCs.

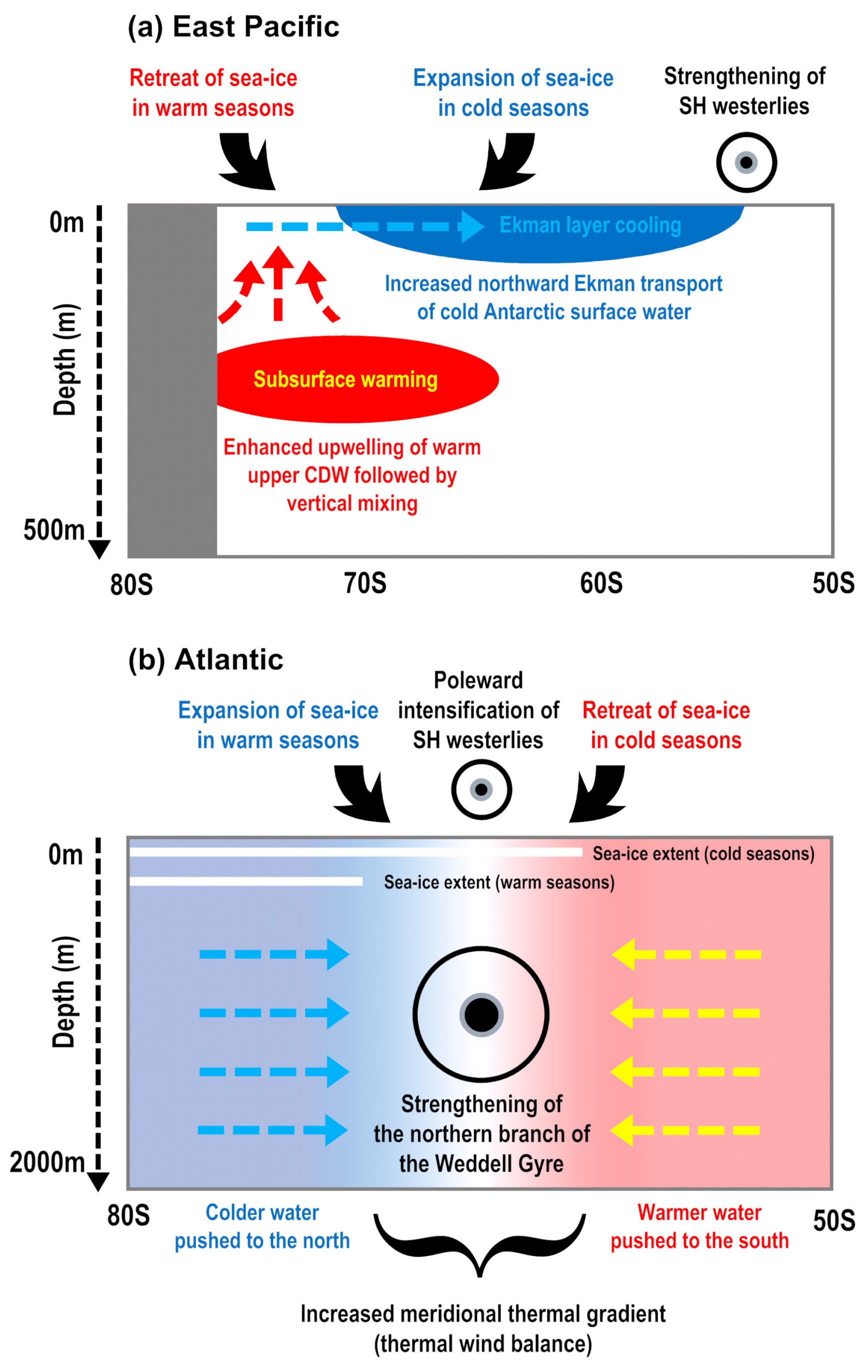

Figure 10. Sketch of the physical mechanisms linking the wind-driven ocean dynamics and the Antarctic sea-ice trends in (a) the East Pacific and (b) Atlantic. In the East Pacific, the strengthening SH westerlies enhanced Ekman upwelling of the warm upper CDW and increased the northward Ekman transport of cold Antarctic surface water, thus contributing to the expansion of sea-ice in the cold seasons and to the retreat in the warm seasons. In the Atlantic, the poleward intensification of SH westerlies strengthened the northern branch of the Weddell Gyre. Constrained by the thermal wind balance, the meridional thermal gradient increased across

the northern branch of the Weddell Gyre, cooling the water column within the Weddell Gyre and warming the water column to the north of the Weddell Gyre, thus contributing to the expansion of sea-ice within the Weddell Gyre in the warm seasons, and to the retreat north of the Weddell Gyre in the cold seasons.